Research paper

Interactions between neutrophil extracellular traps and activated platelets enhance procoagulant activity in acute stroke patients with ICA occlusion

Peng Zhou[a,b], Tao Li[c], Jiaqi Jin[a], Yingmiao Liu[d], Baorong Li[d], Quanye Sun[e], Jiawei Tian[a], Hongtao Zhao[a], Zhihui Liu[a], Shuai Ma[a], Shuoqi Zhang[f], Valerie A Novakovic[g], Jialan Shi[c,h,**], Shaoshan Hu[a,*]

[a] Department of Neurosurgery, The Second Affiliated Hospital, Harbin Medical University, Harbin, PR China
[b] The Key Laboratory of Myocardial Ischemia, Ministry of Education, Heilongjiang Province, Harbin, PR China
[c] Department of Hematology, The First Affiliated Hospital, Harbin Medical University, Harbin, PR China
[d] Department of Stomatology, The First Affiliated Hospital, Harbin Medical University, Harbin, PR China
[e] Department of Clinical Laboratory, Qingdao Municipal Hospital Group, Qingdao, PR China
[f] Department of Neurology, The Second Affiliated Hospital, Harbin Medical University, Harbin, PR China
[g] Department of Research, Brigham and Women's Hospital, VA Boston Healthcare System, Harvard Medical School, Boston, MA, USA
[h] Department of Surgery, Brigham and Women's Hospital, VA Boston Healthcare System, Harvard Medical School, Boston, MA, USA

ARTICLE INFO

ABSTRACT

Background: The role of neutrophil extracellular traps (NETs) in procoagulant activity (PCA) in stroke patients caused by thromboembolic occlusion of the internal carotid artery (ICA) remains unclear. Our objectives were to evaluate the critical role of NETs in the induction of hypercoagulability in stroke and to identify the functional significance of NETs during atherothrombosis.

Methods: The levels of NETs, activated platelets (PLTs), and PLT-derived microparticles (PMPs) were detected in the plasma of 55 stroke patients and 35 healthy controls. NET formation and thrombi were analysed using immunofluorescence. Exposed phosphatidylserine (PS) was evaluated with flow cytometry and confocal microscopy. PCA was analysed using purified coagulation complex, thrombin, and fibrin formation assays.

Findings: The plasma levels of NETs, activated PLTs, and PMP markers in the carotid lesion site (CLS) were significantly higher than those in the aortic blood. NETs were decorated with PS in thrombi and the CLS plasma of ICA occlusion patients. Notably, the complementary roles of CLS plasma and thrombin-activated PLTs were required for NET formation and subsequent PS exposure. PS-bearing NETs provided functional platforms for PMPs and coagulation factor deposition and thus increased thrombin and fibrin formation. DNase I and lactadherin markedly inhibited these effects. In addition, NETs were cytotoxic to endothelial cells, converting these cells to a procoagulant phenotype. Sivelestat, anti-MMP9 antibody, and activated protein C (APC) blocked this cytotoxicity by 25%, 39%, or 52%, respectively.

Interpretation: NETs played a pivotal role in the hypercoagulability of stroke patients. Strategies that prevent NET formation may offer a potential therapeutic strategy for thromboembolism interventions.

Funding: This study was supported by grants from the National Natural Science Foundation of China (61575058, 81873433 and 81670128) and Graduate Innovation Fund of Harbin Medical University (YJSKYCX2018-58HYD).

* Corresponding author: Shaoshan Hu, MD, PhD., Department of Neurosurgery, The Second Affiliated Hospital, Harbin Medical University, 246 Xuefu Road, Nangang District, Harbin 150001, China
** Jialan Shi, MD, PhD., Department of Hematology, The First Affiliated Hospital, Harbin Medical University, 23 Youzheng Street, Nangang District, Harbin 150001, China; Department of Surgery, Brigham and Women's Hospital, VA Boston Healthcare System, Harvard Medical School, 1400 VFW Parkway, West Roxbury, MA 02132, USA.
E-mail addresses: shaoshanhu421@126.com (S. Hu), jialan_shi@hms.harvard.edu (J. Shi).

1. Introduction

Rupture of atherosclerotic plaque and subsequent atherothrombosis are the pathological hallmarks of acute ischemic stroke (AIS). Approximately 29%−56% of AIS patients with intracranial large artery occlusion continue to suffer from severe disability and mortality at a 3-month follow-up [1−3]. Current studies have reported that the levels of coagulation factors and markers (D-dimer, fibrinogen and

Research in context

Evidence before this study

Despite modern advances in pharmacological and interventional therapy, arterial thrombotic complications in acute ischemic stroke (AIS) remain one of its most significant clinical burdens while little is known about the underlying mechanism. Recently, the ability of neutrophils to generate neutrophil extracellular traps (NETs) has offered a novel avenue to connect neutrophils with thromboinflammation. The presence of NETs in thrombi or plasma of AIS patients has been reported. However, these studies did not address the questions of whether and how NETs promote coagulation, and the relationship between NETs, phosphatidylserine positive (PS⁺) platelets, platelet-derived microparticles (PMPs), and endothelial cells.

Added value of this study

In this study, we investigated neutrophils recruited at the site of plaque rupture during internal carotid artery (ICA) occlusion, become activated following platelet-neutrophil interactions and release NETs decorated with functional PS. Our results also showed that PMPs and clotting factors adhere to NETs, demonstrating that NET structures contribute to the formation of thrombin and fibrin in stroke patients, and thus constitute an assembly platform for atherothrombosis. In addition, NET-associated proteases and histones can propagate and amplify endothelial barrier dysfunction and induce a procoagulant phenotype through the induction of PS exposure and tissue factor (TF) expression in endothelial cells.

Implications of all the available evidence

NET formation played a pivotal role in the hypercoagulability and acute thrombotic complications in AIS patients with ICA occlusion. The blockage of NET formation or local neutralization of NET-mediated PS exposure may offer a candidate therapeutic strategy. In addition, future therapeutic strategies could focus on combined strategies directed against NETs with classical anticoagulant drugs to further reduce the risk of thrombosis.

Willebrand Factor (vWF) and histones [13], serving as a scaffold for PLT adhesion, activation, and aggregation. Moreover, our previous study showed that PLTs were frequently activated in AIS patients, as shown by an increased number of phosphatidylserine-positive (PS⁺) cells and by the enhanced release of PLT-derived microparticles (PMPs) [6]. Nevertheless, relatively little is known about the interactions between NETs, PLTs and PMPs and their contribution to the activation of the coagulation cascade in stroke patients. In addition, histological research has shown the presence of NETs in complicated atherothrombotic plaques due to erosion, rupture, or intraplaque hemorrhage [19]. The cytotoxicity of NETs, which leads to endothelial cell (EC) apoptosis and detachment, has been found in superficially eroded plaques [20,21]. However, how NETs lead to EC activation and augment plaque thrombogenicity needs to be further investigated.

In this study, we investigated the differences in neutrophils that release NETs and expose PS from the aortic or carotid lesion site (CLS) blood samples, evaluated the intricate interactions between activated PLTs, PMPs and NETs, and assessed the contribution of NET-PMP complexes to procoagulant activity (PCA) in stroke patients with internal carotid artery (ICA) occlusion. Furthermore, this study characterised a novel mechanism by which NETs can propagate and amplify endothelial barrier dysfunction and induce a procoagulant phenotype. These new findings enabled us to believe that NETs may play a critical role in the PCA of ICA occlusion patients, providing a promising therapeutic strategy for preventing a pathologic hypercoagulable state and reocclusion in stroke patients with ICA occlusion.

2. Materials and methods

2.1. Patients and procedures

Between April 2017 and March 2019, 55 AIS patients with acute ICA occlusion who had undergone endovascular thrombectomy and 35 control individuals with normal carotid angiograms on digital subtraction angiography (DSA) were recruited to this study. The inclusion criteria included the following: patients aged 18 to 85 years, National Institutes of Health Stroke Scale (NIHSS) score (8−25), time from symptoms onset to endovascular thrombectomy within 8 h, modified Rankin Scale (mRS) ≤1, and core infarct volume < 50 mL on magnetic resonance imaging or Alberta Stroke Program Early Computed Tomography Score (ASPECTS) ≥6. Key exclusion criteria included: previous stroke within 30 days, unknown time of symptom onset, associated myocardial infarction or severe infection (sepsis or endocarditis), any known haemorrhagic or coagulation deficiency, and stenosis or any occlusion in a proximal vessel that prevented access to the site of occlusion. All patients were diagnosed at The Second Affiliated Hospital of Harbin Medical University and received antiplatelet therapy after admission. The local ethics committee of Harbin Medical University approved this protocol. All procedures were performed in accordance with the Declaration of Helsinki. All study participants provided written informed consent.

The systemic blood of healthy control subjects was drawn from the femoral sheath during DSA. Two arterial blood samples were sequentially obtained from each ICA occlusion patient: one was from the descending aorta (aortic samples), and the other was from the culprit carotid artery during stent-retriever thrombectomy (CLS samples). Briefly, a 6-Fr long sheath was initially placed into the descending aorta. Aortic samples were obtained from here. After the first 10 mL of blood was discarded, a 15 mL sample was collected. Subsequently, an 8-Fr balloon guiding catheter was placed in the proximal ICA. A Rebar 18 microcatheter (ev3 Inc, Irvine, CA, USA) was advanced up to or past the thrombus over the microwire. Afterwards, aspiration (either manual or with a pump) was performed through the microcatheter. A second 15 mL blood sample surrounding the thrombus was collected during multiple, slow passes through the

microparticles) were increased in AIS [4−6]. However, the exact mechanisms of atherothrombosis, especially in regard to the hypercoagulability of AIS, are still not entirely understood. In addition, due to the limited understanding of the underlying pathophysiology, all the currently available antithrombotic therapies are accompanied by inevitable bleeding risk [7]. Therefore, the development of effective treatments and targets to prevent or treat atherothrombosis in AIS patients is urgently needed.

Among many inflammatory cells and coagulation mediators that promote thrombosis, increasing evidence supports the vital role of polymorphonuclear neutrophils (PMNs) and neutrophil extracellular traps (NETs) in inflammation-associated thrombotic disorders [8−10]. However, the role of neutrophils in cerebral artery thrombosis has been explored very little. Recently, neutrophil counts were found to be associated with an increased risk of stroke recurrence, poor outcomes, and downstream microvascular thromboinflammation [11,12]. Furthermore, the presence of NETs in the thrombi or plasma of patients with AIS was reported [13−15]. However, these studies did not address whether and how NETs promoted coagulation and how NETs contributed to hypercoagulability.

Current studies have reported that platelets (PLTs) are indispensable for NET formation through cell-cell contact or soluble mediators [16−18]. In turn, NET structures contain tissue factor (TF) [9], von

thrombotic material. Next, the guidewire was exchanged for the embolectomy device, and then a stent retriever (Solitaire™ AB device, ev3 Inc, Irvine, CA, USA) was advanced and deployed with the distal portion of the stent placed a few millimetres distal to the thrombus. The stent was kept deployed for 5 min before retrieving it. Whole-blood samples and thrombus material were collected and processed for further research.

2.2. Sample preparation

We isolated human neutrophils by density gradient centrifugation using a neutrophil separation solution kit (TBDsciences, Tianjin, China). Neutrophil purity and viability for all experiments were > 98%. Plasma (platelet-free plasma, PFP) was isolated from blood samples after initial centrifugation at 1000 g for 10 min, followed by the centrifugation of the supernatant at 15,000 g for 20 min; samples were stored at −80 °C. PLTs were isolated, as previously described [9]. Briefly, blood was centrifuged at 150 g for 15 min. Most (75%) of the top layer was removed and centrifuged at 600 g for 15 min at room temperature. After centrifugation, PLTs were resuspended in HEPES buffer for the in vitro study. PMPs were prepared as previously described [22].

Thrombus material collected from multiple passes of one patient was pooled and further considered as one thrombus. Of the 55 collected thrombi, nine were excluded because insufficient material was available to perform the analysis. In each instance, in vitro clots produced with the aortic samples from the same patient served as a reference thrombus material. After retrieval, thrombi were immediately transferred to 4% paraformaldehyde and were paraffinised within 48 h.

2.3. Stimulation and inhibition of NET formation

Neutrophils, isolated either from patients with ICA occlusion or healthy controls, were cultured in RPMI-1640 medium supplemented with 2% healthy individual serum (37 °C, 5% CO_2). For in vitro studies, control neutrophils were stimulated with 5% plasma isolated from ICA occlusion patients or control individuals for 3 h (37 °C, 5% CO_2). In order to explore the role of PLTs, we incubated control neutrophils with PLTs at a ratio of 1:50 for 3 h. In separate experiments, control PLTs were treated with 5% plasma isolated from ICA occlusion patients or from control individuals for 30 min (37 °C, 5% CO_2). For the two-step stimulation of neutrophils, PLTs were pretreated with 5% CLS plasma from ICA occlusion patients (activated PLTs) for 30 min, washed and added to neutrophil cultures with or without 5% CLS plasma from ICA occlusion patients. For interruption of the protease-activated receptor 1 (PAR-1) signaling pathway, PLTs were treated with FLLRN peptide (500 mM) for 30 min. For thrombin inhibition, CLS plasma from ICA occlusion patients was treated with anti-thrombin III (AT-III) or hirudin for 30 min. The control PLT stimulation was performed with recombinant thrombin (0.01 U) as a positive control group [9].

2.4. NET generation, isolation and quantification

NET generation and isolation were performed as previously, with slight modifications [9]. Briefly, 2×10^5 ex vivo or in vitro-stimulated neutrophils were seeded in 6-well plates and incubated for 3 h (37 °C, 5% CO_2). Subsequently, the culture medium was discarded, and cells were washed three times with RPMI-1640. To collect NET structures, we added 2 mL of RPMI-1640 to each per well and collected NETs (the smear on the wells) in 15 mL tubes by vigorous agitation. After being centrifuged for 10 min at 450 g at 4 °C, neutrophils, cellular debris, and any remaining cells would pellet at the bottom, leaving a NET-rich supernatant [23]. The supernatant phase containing NETs was collected and directly subjected to different treatments, including thrombin-antithrombin (TAT) complex, fibrin formation, and endothelial stimulation assays. Quantification of DNA in NET was performed using

Sytox green nucleic acid labeling (Thermo Fisher Scientific, Waltham, MA, USA) [20,21].

2.5. Measurement of NET-DNA complexes and cell-free DNA (cfDNA)

NET-DNA complexes, including myeloperoxidase-DNA (MPO-DNA), neutrophil elastase-DNA (NE-DNA), and citrullinated histone 3-DNA (H3Cit-DNA) complexes, were quantified using capture ELISAs [24,25]. Briefly, NETs were subjected to complete digestion by 10 U/mL DNase I (Sigma-Aldrich, St. Louis, MO, USA) for 20 min at 37 °C. Ethylene Diamine Tetraacetic Acid (EDTA 5 mM) was used to inhibit DNase I activity. Subsequently, supernatants were collected, centrifuged and diluted 20-fold in PBS. Diluted DNase I-digested supernatants were added to 96-well microplates (75 μL per well) pretreated with anti-human MPO (Abcam, Cambridge, UK, Cat# ab25989, RRID: AB_448,948), anti-human NE (Abcam, Cat# ab21595, RRID: AB_446,409), or anti-human H3Cit (Abcam Cat# ab5103, RRID: AB_304,752) overnight at 4 °C. After blocking with 1% bovine serum albumin (BSA,125 μL per well), 40 μL of patient plasma was added per well in combination with the peroxidase-labelled anti-DNA. After 1 h of incubation on a shaking device (320 rpm) at room temperature, the samples were washed with 150 μL of phosphate-buffered saline (PBS) per well, and the TMB substrate was added. The absorbance at 405 nm was calculated after addition of the stop reagent at 37 °C in the dark. cfDNA was detected by a Quant-iT PicoGreen dsDNA Assay Kit (Invitrogen, Carlsbad, CA, USA) according to the manufacturer's instructions [26].

2.6. Assays of the adhesion of PMPs and coagulation factors to NETs

The adhesion of PMPs to NETs was evaluated as previously described with slight modifications [27]. Briefly, platelet-rich plasma (PRP) was obtained from healthy controls by centrifuged blood samples for 15 min at 150 g. The pellet containing platelets was removed from PRP after centrifugation at 710 g for 15 min and was resuspended with Tyrode's buffer at 3×10^8/mL. Thrombin (0.01 U/mL) was added to stimulate PLTs (30 min, 37 °C). After the addition of EDTA, whole platelets were removed by centrifugation (1250 g, 10 min). To isolate PMPs, this solution was centrifuged at 20,000 g (30 min). Control neutrophils were stimulated with 25 nM phorbol 12-myristate 13-acetate (PMA) for 3 h (37 °C, 5% CO_2) and were then incubated with PMPs for 10 min (37 °C). After being fixed by 4% paraformaldehyde, washing with PBS, and blocking with 2% BSA, the preparation was stained with anti-CD41a (BD Biosciences, San Jose, CA, USA, Cat# 347,407, RRID: AB_10,822,936). Secondary antibodies conjugated to Alexa Fluor 555 was used (Invitrogen). Nuclear DNA was stained with (4′,6-diamidino-2-phenylindole) DAPI. For the inhibition experiments, NETs were pretreated with APC (50 nM) for 60 min or DNase I (50 U/mL) for 30 min (37 °C) prior to their incubation with PMPs, or PMPs suspensions were preincubated with lactadherin (128 nM) prior to the assay.

The coagulation factors in plasma binding to neutrophils during NET formation were detected as previously described [28]. After being stimulated with 25 nM PMA for 3 h, neutrophils were incubated with plasma for 15 min (37 °C, 5% CO_2). Coagulation factors and NETs were stained with anti-fibrinogen (1:100, Abcam Cat# ab34269, RRID: AB_732,367), anti-prothrombin (25 μg/mL, Abcam, Cat# ab208589), anti-Factor X (25 μg/mL, Abcam, Cat# ab79929, RRID: AB_1,658,723), or anti-H3Cit (1:100) and were then incubated with Alexa Fluor 488- and 555-conjugated secondary antibodies (Invitrogen). DAPI was used to stain nuclear DNA. For inhibition assays, cells were pre-treated with DNase I (50 U/mL), APC (50 nM) or lactadherin (128 nM) for 1 h at 37 °C before incubation with coagulation factors.

The visualization was performed with a fluorescence microscope. A custom MATLAB program (MathWorks, Natick, MA, USA) was used to analyze immunofluorescence images.

2.7. TAT complex assay and fibrin formation assays

The thrombin concentration was measured in *ex vivo* plasma obtained from the blood of the CLS and aorta from patients with ICA occlusion or from control individuals as previously described with slight modifications [9]. The TAT complex was further detected in control plasma, which was stimulated *in vitro* with NET-PMP complexes, as previously described [9]. In brief, NET structures were isolated from neutrophils and incubated with PMPs for 10 min at 37 °C. Next, NET-PMP complexes were incubated for 10 min (37 °C) and mixed with plasma at a ratio of 1:5. After incubation, the plasma mixture was immediately transferred to ice to prevent further thrombin activation. For inhibition assays, NET-PMP complexes were pretreated with DNase I (100 U/mL) for 25 min, a neutralizing anti-TF antibody (40 µg/mL, Abcam Cat# ab48647, RRID: AB_870,660) for 10 min or lactadherin (128 nM) for 15 min at 37 °C before plasma stimulation. TAT complex was calculated following the manufacturer's instructions (Siemens Healthcare Diagnostics, Deerfield, IL, USA). *Ex vivo* measurements are depicted as ng/mL, while *in vitro* plasma stimulations are represented as a percentage of increase compared to the control. Quantification of fibrin formation by turbidity was performed [6,29]. Isolated PMPs and NETs were added to re-calcified (10 mM, final) microparticle-depleted plasma (MDP, 88%, final) isolated from healthy controls with or without DNase I (100 U/mL) or lactadherin (128 nM). Fibrin formation was calculated at 405 nm in a SpectraMax 340 PC plate reader [29].

2.8. Endothelial stimulation and inhibition assays

Human umbilical vein ECs (HUVECs) (RRID: CVCL_2959) were incubated in EC medium with or without different concentrations of NETs that were released by neutrophils for different time intervals at 37 °C in 5% CO_2. For inhibition assays, isolated NETs were pretreated with an anti-MMP9 antibody (1 µg/mL, Abcam Cat# ab38898, RRID: AB_776,512), sivelestat (100 nM, S7198, Sigma-Aldrich, a selective inhibitor of elastase), or activated protein C (APC, 100 nM, Sigma-Aldrich) for 1 h (37 °C), and then were added into the supernatant of HUVECs. Vascular cell adhesion molecule-1 (VCAM-1) and intercellular adhesion molecule-1 (ICAM-1) expression were analysed by ELISA and western blotting. Flow cytometry was used to measure the expression levels of CD31, VE-cadherin, ZO-1, and PS. Intrinsic Factor Xa (FXa), prothrombinase, and extrinsic FXa assays were also performed [6].

2.9. Flow cytometric analysis

After isolation and *in vitro* stimulations, Alexa Fluor 488-labelled lactadherin with was used to stain PS exposure on PLTs. PLTs were stained for surface activation markers with fluorescein-labelled anti-CD62P (Abcam Cat# ab6632, RRID: AB_2,184,964) or phycoerythrin (PE)-conjugated anti-CD41a antibody (BD Biosciences). PMPs were identified as previously reported [6]. Briefly, to isolate the MPs, 250 µL of PFP was thawed on ice for 60 min and then centrifuged for 30 min at 20,000 g at 20 °C. Subsequently, 225 µL of MDP were removed, and the remaining 25 µL MPs pellet was harvested. Next, 5 µL of MPs-enriched suspension was resuspended in 35 µL Tyrode's buffer and incubated with Alexa Fluro 488-conjugated lactadherin and PE-conjugated CD41a antibody; Alexa Fluro 488 or Alexa Fluro 647-conjugated IgG2a/IgG1 isotype controls (5 µL) together with beads (1 µm) in a Truecount Tube for 30 min at 4 °C in the dark. Finally, PMPs were calculated by flow cytometric analysis. Truecount Tube calculated the number of PMPs (per µL) after an accumulation of 10,000 gated events. Neutrophils were specifically stained with anti-CD66b (BD Biosciences Cat# 561,927, RRID: AB_10,924,589). PS exposure on neutrophils was stained with Alexa Fluor 488-labelled lactadherin. Identification of neutrophil-platelet aggregates was performed as previously reported [9,30]. In brief, blood samples were stained with Alexa Fluor 488-conjugated anti-CD66b for neutrophils and PE-conjugated anti-CD41a for platelets at 4 °C for 30 min. The neutrophil-platelet aggregates were defined as the increased PE fluorescence intensity within the CD66b+ population region. Flow cytometry was performed using a BD Biosciences FACSort flow cytometer, and data were analysed with FlowJo software (Treestar).

2.10. Western blot analysis

Whole-cell lysates from 15,000 ECs were subjected to 8% gradient SDS-PAGE, and the proteins were transferred onto nitrocellulose membranes. Blots were blocked with 5% defatted milk and incubated with the appropriate primary antibodies overnight at 4 °C, followed by HRP-conjugated secondary antibodies at room temperature for 2 h. Membranes were developed using a chemiluminescence reagent (Thermo Fisher Scientific) [20,31]. The primary antibodies were: anti-ICAM-1 (Cat# Ig60229-1-Ig, Proteintech, Chicago, IL, USA), anti-β-actin (Sigma-Aldrich Cat# A1978, RRID: AB_476,692), anti-VCAM-1 (Proteintech Cat# 11,444−1-AP, RRID: AB_2,214,232), anti-CD31 (BD Biosciences Cat# 560,983, RRID: AB_10,562,393), and anti-VE-cadherin (Abcam Cat# ab33168, RRID: AB_870,662).

2.11. Real-time quantitative PCR

Total RNA isolation and cDNA synthesis were performed as previously reported [31]. Real-time quantitative PCR for TF in HUVECs was conducted as previously described [20]. The primer sequences were GAPDH, 5′-AATGAAGGGGTCATTGATGG-3′ and 5′-GAAGGTGAAGGTCG-GAGTCA-3′; and TF, 5′-TGACTTAGTGCTTATTTGAACAGTG-3′ and 5′-GTCTTCGCCCAGGTGGC-3′.

2.12. Immunofluorescence and confocal microscopy

Cells and thrombi were prepared as previously reported [10,14,32]. NETs were stained using anti-NE, anti-MPO, anti-MMP9, or anti-H3Cit. Alexa Fluor 488-lactadherin was used for PS staining in NETs, PLTs, or HUVECs. Thrombus sections were stained with anti-CD66b, anti-H3Cit, or Alexa Fluor 488-lactadherin. HUVECs were also stained with antibodies against ZO-1 (Abcam Cat# ab96587, RRID: AB_10,680,012), VE-cadherin (Abcam), TF (Abcam), CD31(Abcam), ICAM-1 (Proteintech), and VCAM-1 (Proteintech). F-actin filaments were stained using tetramethylrhodamine (TRITC)- or fluorescein isothiocyanate (FITC)-conjugated phalloidin. Samples were then incubated with Alexa Fluor 647, 488, or 555-conjugated secondary antibodies (Invitrogen). Nuclei were labelled with propidium iodide (PI) or DAPI. Factor Va (FVa)-fluorescein-maleimide and FXa-EGRck-biotin were used to detect FVa and FXa binding on stimulated HUVECs. To detect fibrin networks on stimulated HUVECs, cells were stained with Alexa Fluor 647-labelled fibrinogen. Images were visualised using immunofluorescence microscopy or confocal microscopy.

2.13. Statistical analysis

All data were analysed by GraphPad Prism 7.0 or SPSS 16.0 statistical software. Values are presented as the mean ± the standard deviation (SD) and are based on at least triplicate measurements. One-way ANOVA or Student's *t*-test was used for statistical analysis as appropriate. Correlation between two variables was analysed using the Spearman rank correlation test. Results were considered statistically significant when *P*-value < 0.05.

3. Results

3.1. Subject characteristics

The characteristics of healthy subjects and stroke patients with ICA occlusion are summarized in Table 1. The two groups were similar with respect to major clinical and laboratory characteristics. However, levels of D-dimer, fibrinogen, and C-reactive protein were higher in stroke patients than in healthy controls, suggesting a hypercoagulable state in stroke patients with ICA occlusion. Additionally, compared with healthy controls, neutrophil counts were also higher in patients.

3.2. NETs accumulated at the CLS in stroke patients with ICA occlusion

A schematic illustration of aortic and CLS sampling and representative imaging during stent-retriever thrombectomy are shown in Fig. 1a and Supplementary Fig. S1. We observed NET release in *ex vivo* neutrophils isolated from blood samples that were obtained near the CLS aspiration catheter in ICA occlusion patients; a significant difference in the number of NET-releasing cells was found compared with the other groups (Fig. 1b and c). Immunofluorescence microscopy and western blot analysis also confirmed the presence of MMP-9 in NETs in CLS samples (Supplemental Fig. S2). NET-specific markers, including MPO-DNA, H3Cit-DNA, NE-DNA complexes, and cfDNA were also elevated in the plasma obtained from CLS samples relative to those from aortic samples or controls (Fig. 1d−g). In addition, cfDNA showed a significant positive correlation with circulating NET-DNA complexes in ICA occlusion patients (Supplemental Fig. S3),

Table 1
Characteristics of the study population.

Characteristics	ICA occlusion (n = 55)	Control (n = 35)	P value
Age, y	65.35 ± 11.5	61.44 ± 9.89	0.675
Gender, M/F	31/24	16/19	0.285
Total cholesterol (mmol/L)	5.59 ± 0.86	3.2 ± 0.56	0.001
Triglycerides (mmol/L)	2.69 ± 0.73	1.40 ± 0.40	0.301
LDL (mmol/L)	3.58 ± 0.83	1.61 ± 0.06	0.002
HDL (mmol/L)	1.34 ± 0.21	0.79 ± 0.08	0.183
C-reactive protein (mg/L)	5.21 ± 2.72	1.16 ± 0.41	0.022
D-dimer (mg/L)	0.68 ± 0.22	0.15 ± 0.03	0.005
Fibrinogen (g/L)	5.02 ± 0.79	2.23 ± 0.43	0.001
APTT (sec)	28.70 ± 2.35	26.18 ± 3.34	0.235
PT (sec)	11.79 ± 0.30	11.4 ± 0.52	0.361
Erythrocytes ($\times 10^{12}$/L)	4.67 ± 0.28	4.29 ± 0.11	0.437
Platelets ($\times 10^{9}$/L)	232.31 ± 1.28	249.29 ± 2.81	0.621
Leukocytes ($\times 10^{9}$/L)	7.58 ± 1.81	5.70 ± 0.48	0.071
Neutrophils (%)	75.38 ± 2.51	63.50 ± 2.82	0.043
Monocytes (%)	6.12 ± 0.62	5.09 ± 0.71	0.623
Lymphocytes (%)	28.19 ± 4.62	25.09 ± 1.79	0.551
Eosinophils (%)	2.9 ± 1.06	2.7 ± 1.19	0.754
Basophils (%)	0.31 ± 0.06	0.28 ± 0.11	0.634
NIHSS score	12 (8−25)	−	NA
Previous AIS or TIA (n)	5	−	NA
Hypercholesterolemia (n)	23	13	0.659
Hypertension (n)	22	12	0.586
Diabetes mellitus (n)	20	12	0.841
Cigarette smoking (n)	21	16	0.479
Pharmacological therapy			
Antiplatelet (n)	15	−	NA
Anticoagulant (n)	6	−	NA
Fibrinolysis (n)	11	−	NA
ACE inhibitor or ARB (n)	19	14	0.601
Statin (n)	18	11	0.898

HDL, high-density lipoprotein; LDL, low-density lipoprotein; APTT, activated partial thromboplastin time; NA, not available; PT, prothrombin time; APTT, activated partial thromboplastin time; ICA, internal carotid artery; NIHCC, National Institutes of Health Stroke Scale; AIS, acute ischemic stroke; TIA, transient ischemic attack. Data expressed as the means ± SD, unless indicated otherwise. P < 0.05 was considered statistically significant.
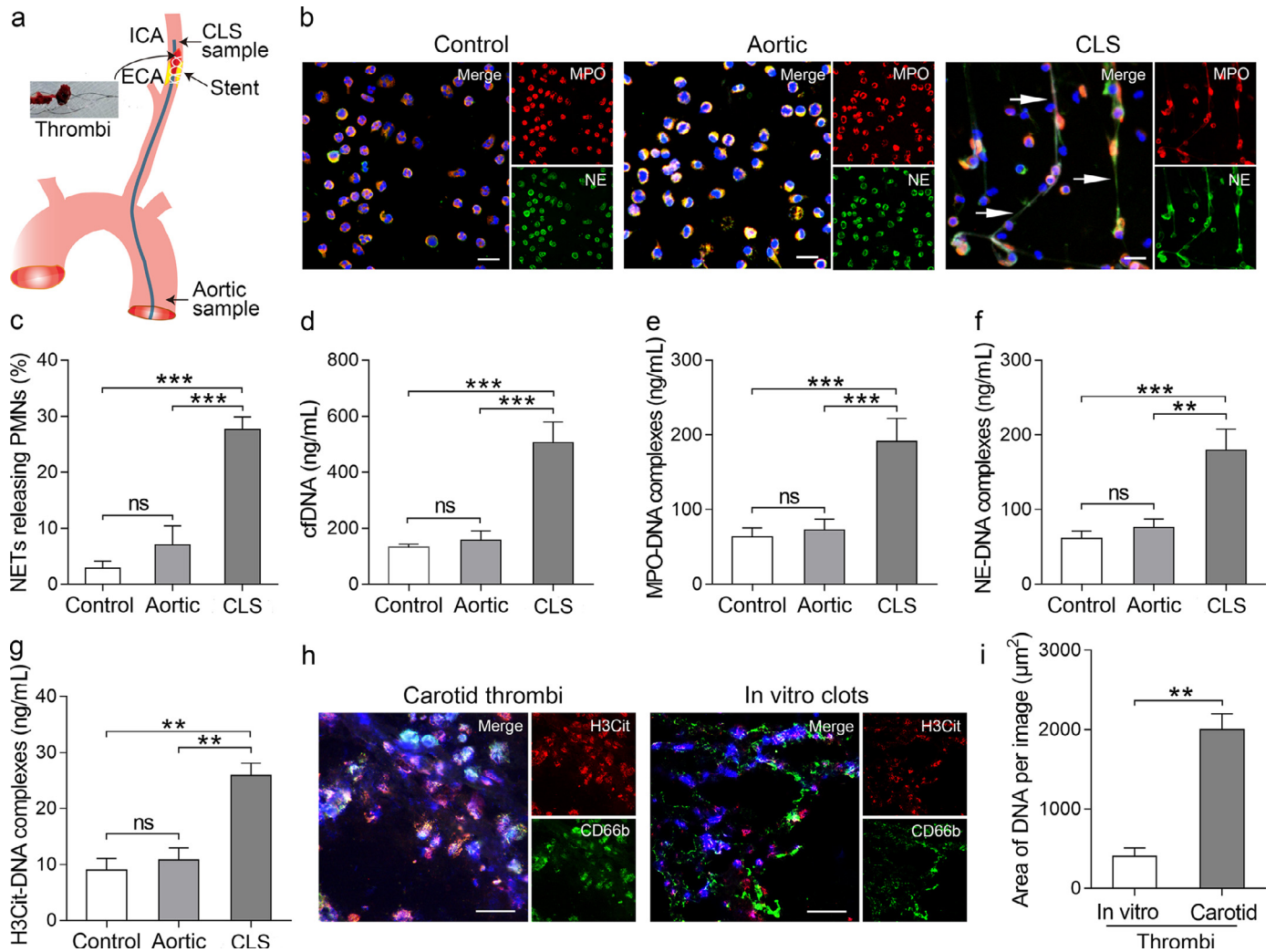
suggesting that the cfDNA is at least partially neutrophil-derived. Furthermore, immunofluorescence staining confirmed that extracellular DNA colocalised with H3Cit and the granulocyte marker CD66b, suggesting that neutrophils and NETs were present in carotid thrombi. In contrast, neutrophils and NETs were not commonly found in vitro clots, which were spontaneously produced in the blood from the same patients (Fig. 1h). Notably, carotid thrombi contained nearly 4-fold more extracellular DNA than in vitro clots (Fig. 1i).

3.3. PS exposure is differentially localised on blood cells of ICA occlusion patients

PS on the surface of MPs and blood cells provides binding sites for the activation of coagulation factors, thus acting as a critical catalyst in the coagulation cascade [6,33,34]. Lactadherin, a selective probe and effective blocker of PS, can be used to detect PS exposure on MPs and to determine their origin more sensitively than annexin V [35−37]. Therefore, we used lactadherin to measure the level of PS exposure on neutrophils and PLTs. As shown in Fig. 2a, control neutrophils showed a normal lobulated nucleus. In contrast, nuclei lost their lobular shape, expanded, and showed diffuse rim staining by lactadherin in aortic samples. In CLS samples, the extracellular DNA of neutrophils formed a meshwork of threads that concurrently stained with lactadherin. Flow cytometry demonstrated that the exposure of PS on neutrophils isolated from both the CLS and aortic samples of ICA occlusion patients was higher than that in samples from healthy individuals (Fig. 2b and Supplemental Fig. S4). The numbers of PS$^+$ PLTs and PMPs detected in the CLS samples were significantly higher than those from the aortic samples and control subjects (Fig. 2c and d). PLTs from the CLS had increased levels of P-selectin (CD62P, Fig. 2e) and platelet/neutrophil aggregates (CD41a$^+$/CD66b$^+$ counts, Fig. 2f) compared with those from the other groups, as observed by flow cytometric analysis. The mean percentage of lactadherin$^+$ PLTs and PMPs, CD62P$^+$ PLTs, and platelet/neutrophil aggregates were showed in Supplemental Table 1. As shown in Fig. 2g, confocal microscopy images demonstrated that control PLTs did not stain with lactadherin, while robust lactadherin binding was observed on PLT membranes from CLS samples. Moreover, carotid thrombi showed NETs and PS localization, as observed by lactadherin/H3Cit costaining by immunofluorescence microscopy, whereas PS was rarely detected in vitro clots (Fig. 2h).

The local NET formation and PS exposure at the CLS of ICA occlusion patients suggest that they are possibly critical players in the hypercoagulability of this disease. Next, we aimed to investigate whether the circulatory microenvironment of ICA occlusion can induce NETosis and PS exposure on neutrophils.

3.4. CLS plasma induces PS exposure but not NETosis

First, we assessed the effect of plasma from ICA occlusion patients on PS exposure. Neutrophils treated with CLS or aortic plasma showed a higher increase in PS exposure than neutrophils treated with plasma from control individuals (Fig. 3a and b). Next, we evaluated the effect of plasma from different sources on NET release. However, no significant increase in NET generation was detected (Fig. 3c and d). We further observed that CLS plasma could increase the activation of control PLTs, whereas aortic-derived or control plasma could not, as demonstrate by lactadherin and CD62P flow cytometry analysis (Fig. 3e, P < 0.01). We also found that the mean percentage of CD41a$^+$ lactadherin$^+$ PLTs in the CLS sample was significantly higher than that in the aortic sample of ICA occlusion patients (Fig. 3f, P < 0.001). Similarly, a significant elevation of PMP levels was observed in the control PLTs following stimulation with plasma from the CLS compared with plasma from the aorta and healthy controls (Fig. 3g).

Since thrombin can activate PLTs through protease-activated receptors (PARs), we examined the effect of thrombin on the

Fig. 1. NETs accumulation at the CLS of patients with ICA occlusion. (a) A schematic drawing of aortic and CLS sampling during stent retriever thrombectomy. (b) Representative immunofluorescence images showed NETs released by PMNs from the CLS, aortic, or control samples. NETs were characterised by NE (green), MPO (red) and DNA (blue). Arrows indicated NETs. (c) Percentage of NET-releasing PMNs in isolated PMNs obtained by selective blood sampling. (d−g) cfDNA, H3Cit-DNA, MPO-DNA, and NE-DNA complexes levels were measured. (h) NETs visualised in carotid thrombi by co-staining of the granulocyte marker CD66b (green) with H3Cit (red) and DNA (blue). In vitro clots with the blood from the same patient served as the reference thrombus material. (i) Images were then analyzed in a custom MATLAB program to quantify each pixel-positive signal as area DNA per image. All values are mean ± SD. One representative out of seven (a) or eight (h) independent experiments is shown. Statistics, one-way ANOVA. **$P < 0.01$, ***$P < 0.001$, ns = not significant. Bars represent 50 μm. For (d−g) control samples, $n = 35$; aortic samples, $n = 55$; CLS samples, $n = 55$. (For interpretation of the references to colour in this figure legend, the reader is referred to the web version of this article.)

activation of CLS PLTs. We first investigated thrombin levels in plasma, as assessed by a TAT complex ELISA. As shown in Fig. 3h, TAT complex levels markedly increased in the CLS plasma in comparison to the aortic or control group plasma. Furthermore, a significantly greater decrease in PLT activation and PS$^+$ PMPs was observed after adding the AT-III (a thrombin inhibitor), hirudin, or specific PAR-1 antagonism, suggesting that PLT activation by CLS plasma was thrombin-dependent (Fig. 3i and j).

3.5. Activated PLTs at the CLS are responsible for NET generation

PLTs are responsible for NET formation in many thrombotic diseases [16,18]. Thus, we examined whether PLTs at the CLS of ICA occlusion patients were responsible for NET formation. Control neutrophils treated with CLS PLTs showed significantly elevated NET release, whereas the treatment of neutrophils with aortic or control PLTs did not promote NET formation (Fig. 4a−c). Interestingly, PS exposure was not observed on NETs generated by activated PLTs when CLS plasma was not added (Fig. 4a). Similar to the CLS PLTs, in vitro-activated PLTs stimulated the production of PS-free NETs by

control neutrophils (Fig. 4d). Furthermore, the generation of NETs in response to PLTs activated with CLS plasma was significantly reduced by the concomitant administration of AT-III, hirudin, or a PAR-1 antagonist (Fig. 4e and f, Supplemental Fig. S5).

We further studied the combined roles of PLTs and plasma in the formation of PS-bearing NETs through a "two-hit" experimental procedure. First, the PS exposure of neutrophils was measured after incubation with CLS plasma from ICA occlusion patients. Then, NET generation was stimulated in these PS$^+$ neutrophils after adding activated PLTs (CLS PLTs or in vitro-activated PLTs), as previously described (Fig. 4g and h).

3.6. NET-PMP complexes at the CLS increase thrombin and fibrin formation

To understand the function of PS-bearing NETs on the PCA of ICA occlusion patients, we explored if PMPs could bind to NETs in vitro and could thus contribute to the enhanced PCA in patients. These results showed that PMPs could adhere to NETs, demonstrating that NETs provide an assembly platform for PMPs (Fig. 5a). The cleavage
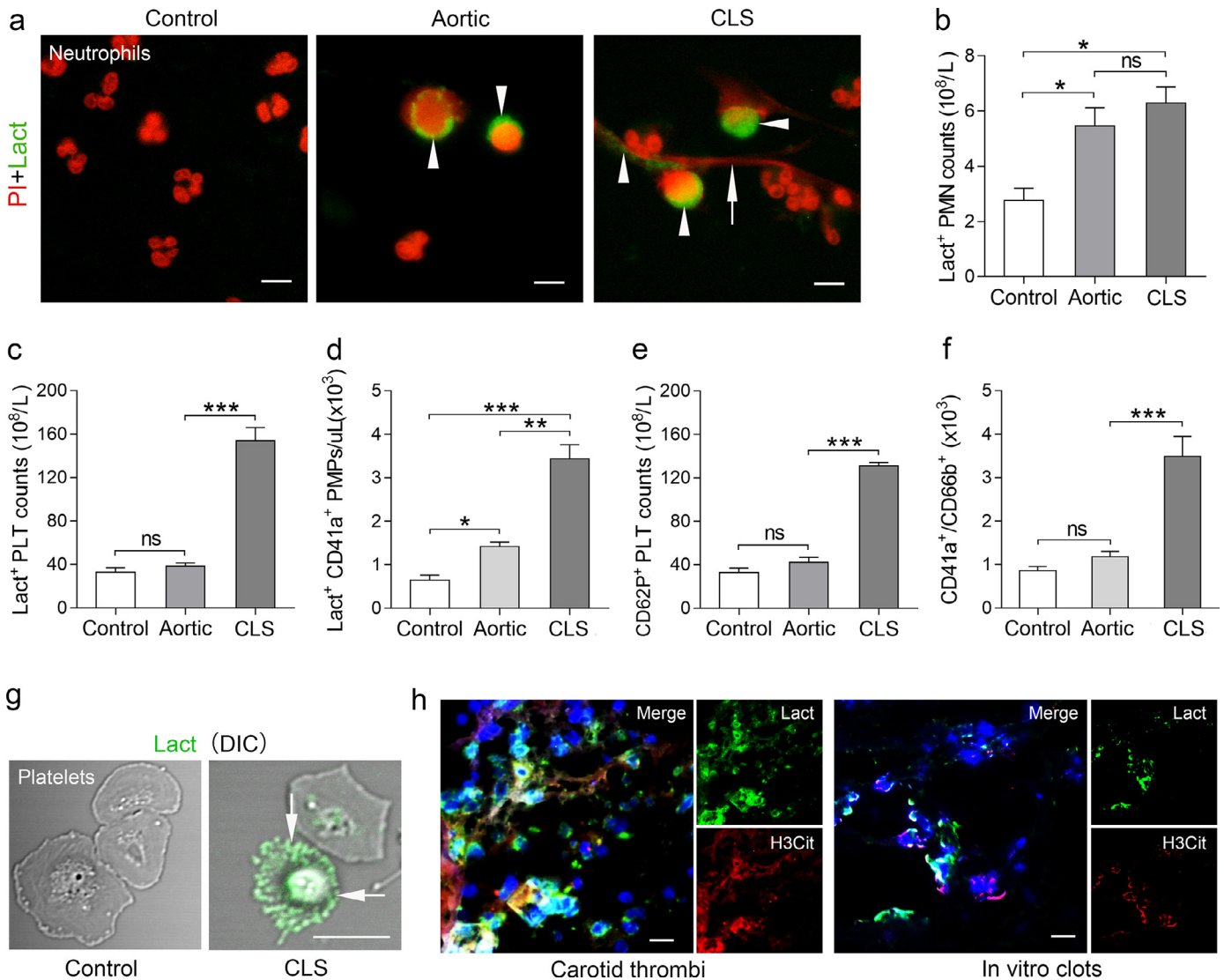
Fig. 2. The quantification and location of PS exposure on PMNs and PLTs. (a) Representative immunofluorescence images showing PMNs obtained from selective blood sampling stained by lactadherin (green) and PI (red). Control PMNs were barely marked with lactadherin. In aortic samples, nuclei of PMNs lost their lobular shape, spilled out of the ruptured cell, and showed diffuse rim staining by lactadherin (arrows). In CLS samples, the extracellular DNA of PMNs formed a meshwork of threads (arrow) and concurrently stained with lactadherin (arrowheads). (b) Lactadherin-binding (PS$^+$) counts of PMNs were measured by flow cytometry. The counts of lactadherin$^+$ PLTs (c), lactadherin$^+$ PMPs (d), and CD62P$^+$ PLTs (e) were measured. (f) Platelet/neutrophil aggregates were defined as CD41a$^+$/CD66b$^+$ per 10,000 CD66b$^+$ events with fluorescence-activated cell-sorting analysis in PMNs. (g) PLTs from control and CLS blood samples were stained with lactadherin (green, arrows) and imaged by confocal microscopy. (h) PS (lactadherin, green) on NETs in thrombi specimens from ICA occlusion patients, was co-localized with H3Cit (red) and DNA (blue). All values are mean ± SD. One representative out of six (a, g) or eight (h) independent experiments is shown. Statistics, one-way ANOVA. *$P < 0.05$, **$P < 0.01$ and ***$P < 0.001$, ns = not significant. Bars represent 50 μm in (a), (h), 5 μm in (g). For (b-f) control samples, $n = 35$; aortic samples, $n = 55$; CLS samples, $n = 55$. (For interpretation of the references to colour in this figure legend, the reader is referred to the web version of this article.)

of histones by APC, the degradation of the DNA scaffold by DNase I or the blockade of PS by lactadherin reduced the degree of PMP adhesion by 64.3%, 56.5%, and 47.5%, respectively (Fig. 5b, $P < 0.01$). We next designed experiments to quantify the binding of endogenous clotting factors to NETs. The binding of coagulation factors (prothrombin, fibrinogen, and Factor X) to NET structures was detected (Fig. 5c), suggesting that these structures served as an assembly site for prothrombinase complexes. We estimated the role of DNA, histones, and PS, which comprise NETs, in the promotion of coagulation factor binding. Similarly, a significantly higher decrease in the degree of coagulation factor adhesion was observed after treatment with DNase I, APC, and lactadherin (Fig. 5d, $P < 0.01$).

Since inhibitors could reduce NET-PMPs or NET-coagulation factor binding, inhibitors may also reduce the prothrombotic phenotype of NETs. When studying the PCA of NET-PMP complexes, we detected markedly increased TAT levels after incubating plasma with NET-PMP complexes obtained from CLS samples compared with NET-PMP

complexes isolated from the other groups (Fig. 5e). The degradation of the chromatin scaffold with DNase I or the blockade of PS with lactadherin decreased thrombin generation by 72% and 65%, respectively. The addition of a neutralizing anti-TF antibody played a minor function (Fig. 5e). Next, we estimated the capacity of NET structures and PMPs to promote fibrin formation. NETs and PMPs from CLS samples caused in significantly more fibrin production than those isolated from the other groups (Fig. 5f, $P < 0.01$). Lactadherin or DNase I effectively inhibited fibrin formation (Fig. 5g, $P < 0.01$), indicating that PS-bearing NETs and PS$^+$ PMPs are both indispensable for the hypercoagulability associated with ICA occlusion.

3.7. NET-associated proteases and histones lead to EC activation

NET formation can activate ECs and can even trigger their death [26], and NETs are associated with apoptotic ECs in human atheroma [21]. Therefore, we wondered whether NETs isolated from the CLS of
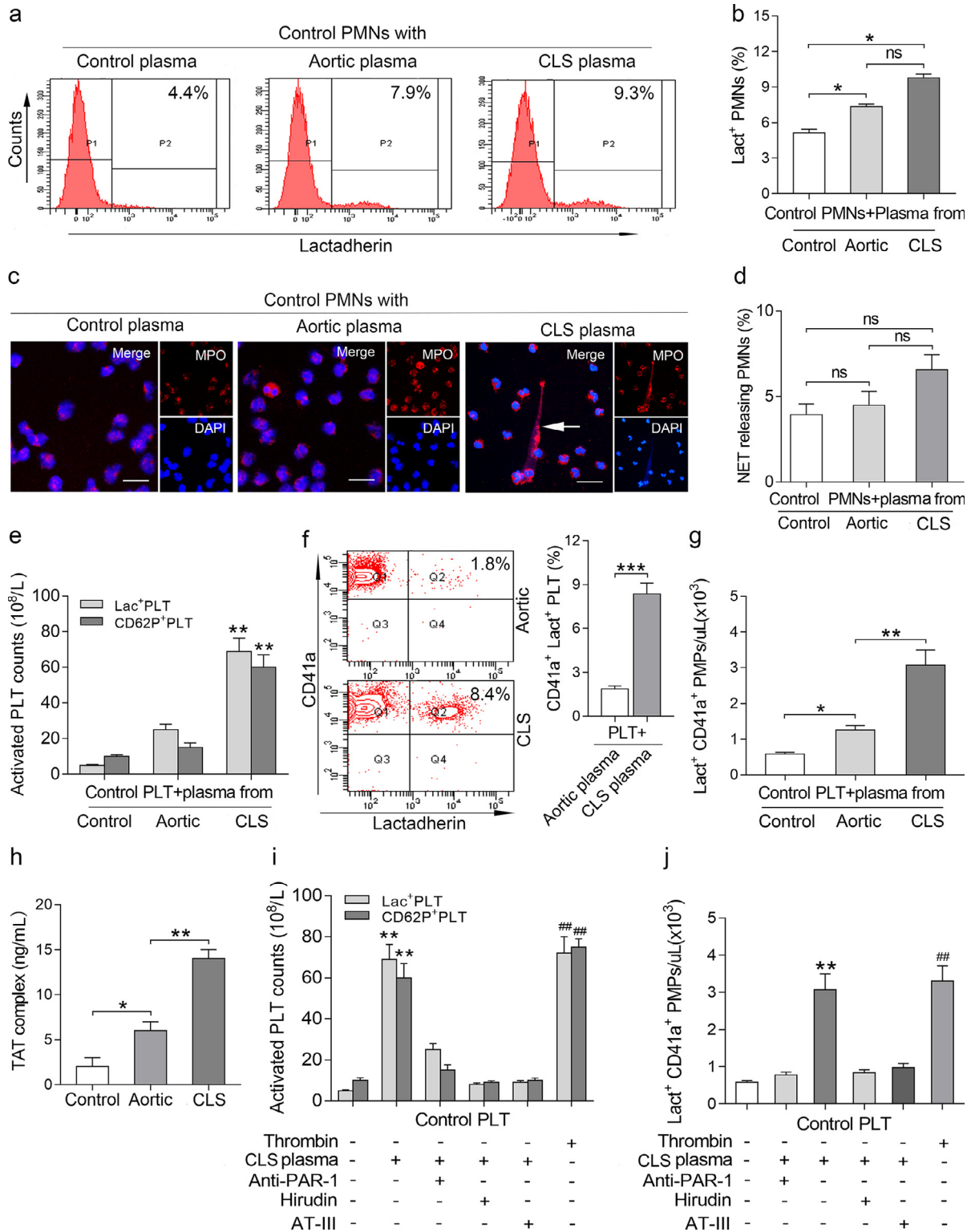
Fig. 3. The microenvironment in ICA occlusion induces PS exposure but not NETs. (a and b) PS exposure of stimulated PMNs was detected by flow cytometry with lactadherin staining. (c) Representative immunofluorescence images of NET generation in control PMNs treated with plasma obtained from the CLS, aortic, or control samples. NETs were stained by MPO (red) and DNA (blue). Arrows indicated NETs. Representative images of five independent experiments are shown. (d) Percentage of NET-releasing PMNs in control PMNs incubated with plasma obtained by selective blood sampling. (e) Flow cytometry analysis of lactadherin and CD62P on control PLTs treated with CLS, aortic, or control plasma. (f) The proportion of activated PLTs (CD41a$^+$ lactadherin$^+$) of the density plots was quantified. (g) Lactadherin$^+$ PMP levels were observed in control PLTs following stimulation of plasma obtained from selective blood sampling. (h) Thrombin levels obtained by selective sampling as assessed by TAT complex ELISA. Control PLTs treated with CLS plasma in the presence or absence of thrombin inhibitors (AT-III or hirudin) and PAR-1 inhibitors. Recombinant thrombin was used as a positive control. Activated PLTs (i) and lactadherin$^+$ PMPs (j) were tested by fluorescence-activated cell-sorting analysis. Scale bar: 50 μm. All values are mean $\pm$ SD. Statistics, one-way ANOVA. $^{\#\#}P < 0.01$, $^{**}P < 0.01$versus control and inhibitor-treated group in (i) and (j), $^*P < 0.05$, $^{***}P < 0.001$, ns = not significant. For (a) (b) (d) n = 17. For (e−j) n = 18. (For interpretation of the references to colour in this figure legend, the reader is referred to the web version of this article.)
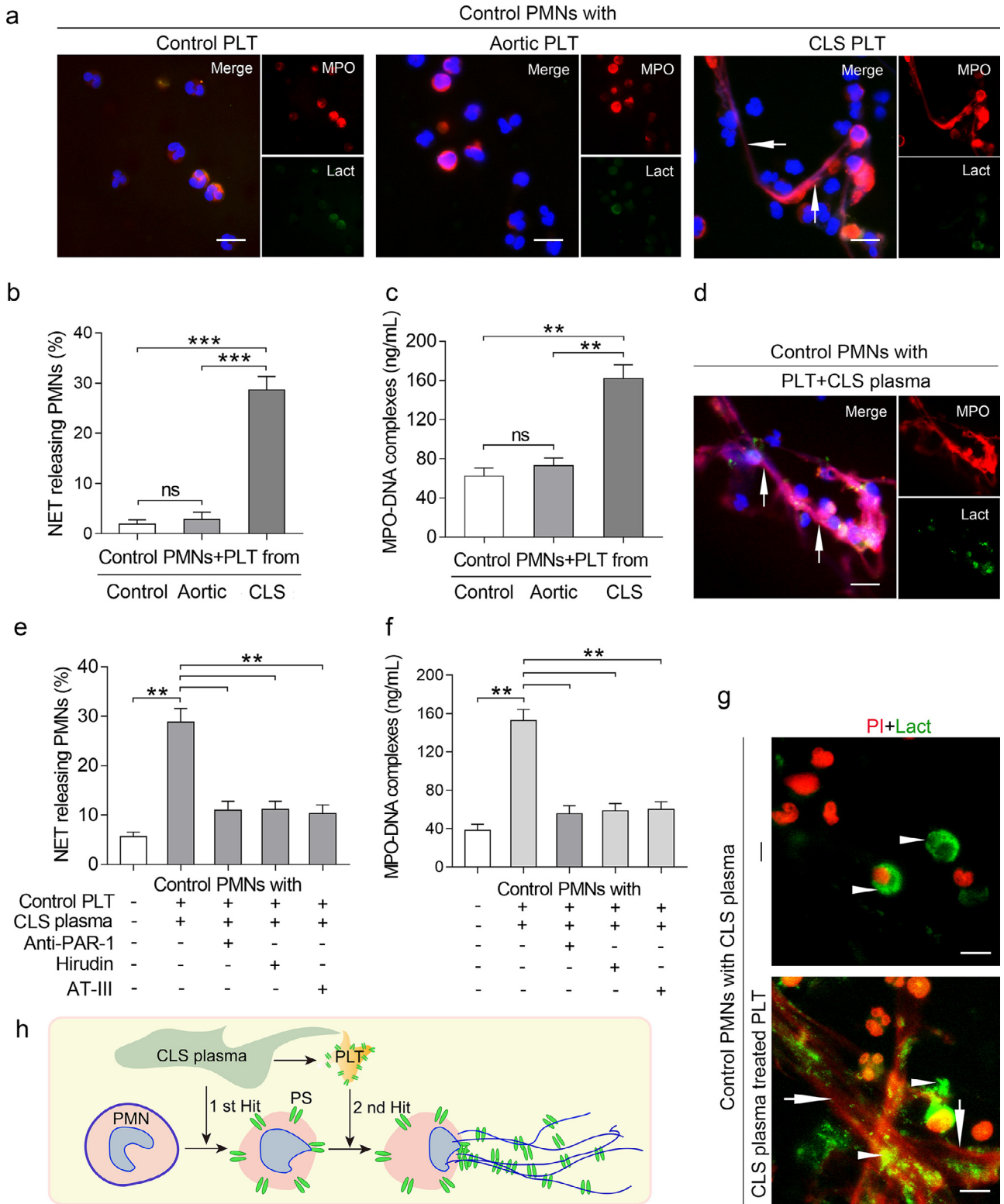
Fig. 4. The role of plasma and PLTs in the formation of PS-bearing NETs. (a) NET generation by control PMNs treated with PLTs isolated from selective blood sampling. The presence of lactadherin (green), MPO (red, arrows) and DAPI (blue) were seen by immunofluorescence microscopy. Representative images of six independent experiments are shown. (b) Quantification of the percentage of NET-releasing PMNs and (c) the concentration of MPO-DNA complex levels in the supernatant after treatment with PLTs isolated from selective blood sampling. PMNs were incubated with unstimulated or CLS plasma-stimulated PLTs in the presence and absence of AT-III, hirudin, or PAR-1 antagonist. (d) Representative images of immunofluorescence staining for PS exposure (lactadherin, green) and NET formation (MPO, red, arrows). (e) The percentage of NET-releasing PMNs, and (f) MPO-DNA complex were evaluated. (g) PS-bearing NET generation after stimulation of control PMNs with CLS plasma and control PLTs pre-treated with CLS plasma. Representative immuno-fluorescence images of PMNs were stained by lactadherin (green) and PI (red). The extracellular DNA spread into the extracellular space (arrows), which co-stained with lactadherin (arrowheads). (h) A model of "two-step" process of generation of PS-binding NETs. All values are mean ± SD. One representative out of six (d) or five (g) independent experiments is shown. Statistics, one-way ANOVA. Scale bar: 20 μm. **$P < 0.01$, ***$P < 0.001$, ns = not significant. For (b) (c) (e) (f) $n = 15$. (For interpretation of the references to colour in this figure legend, the reader is referred to the web version of this article.)
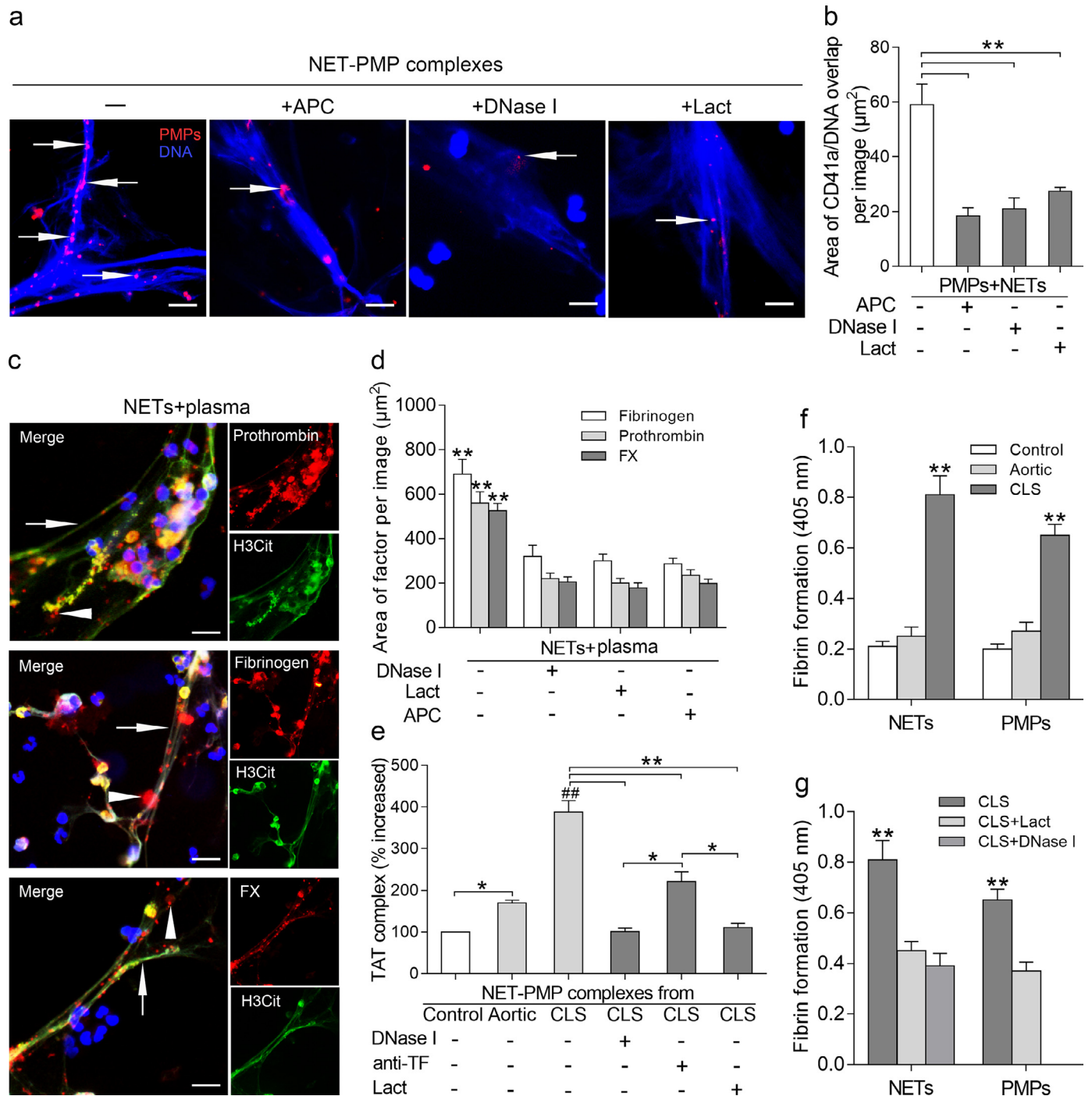
Fig. 5. Formation of NET-PMP complexes and their role in PCA. (a) Representative immunofluorescence images showing PMPs adhere to NETs. PMPs were labeled with CD41a (red, arrows), and extracellular DNA was stained with DAPI (blue). Treatment with APC, DNase I, and lactadherin prevented PMPs adhesion. (b) Immunofluorescence images were analyzed in a custom MATLAB program to quantify each pixel-positive signal as the area of both CD41a and DNA signals per image. (c) Representative immunofluorescence images showing the coagulation factors: prothrombin, fibrinogen, and Factor X (red, arrowheads) binding to NET structures (H3Cit, arrows). (d) For inhibition assays, PMNs were pretreated with lactadherin, DNase I, or APC. Coagulation factors binding NETs were then quantified as area per image. (e) Thrombin levels were analysed with TAT complex ELISA. Thrombin levels in control plasma incubated with isolated NET-PMP complexes from selective blood sampling. Samples were pretreated with DNase I, anti-TF antibody, or lactadherin to prevent thrombin generation. (f) The ability of NET structures and PMPs to support fibrin formation were tested using turbidity measurements. Fibrin polymerisation was monitored at 405 nm. (g) Inhibition of fibrin formation by lactadherin or DNase I were performed using CLS samples. All values are mean ± SD. One representative out of six (a) or four (c) independent experiments is shown. Statistics, one-way ANOVA. Scale bar: 50 μm. **$P < 0.01$ versus control or aortic groups in (f). **$P < 0.01$ versus DNase I or lactadherin treated groups in (g). *$P < 0.05$, **$P < 0.01$. ##$P < 0.01$ versus DNase, lactadherin or APC treated groups in (d), ##$P < 0.01$ versus control or aortic groups in (e). For (d−g) $n = 18$. (For interpretation of the references to colour in this figure legend, the reader is referred to the web version of this article.)

ICA occlusion patients could activate ECs. To test the hypothesis, we evaluated the expression of ICAM-1 and VCAM-1 in HUVECs exposed to various concentrations of NETs for different time intervals. At a high NET concentration (0.5 μg DNA/mL), both VCAM-1 and ICAM-1 expression levels increased after 12 h and reached a maximum at 24 h (Fig. 6a−d). Since EC adherence and endothelial integrity rely on junctional proteins, we further assessed the expression of the intercellular (junctional) proteins CD31 and VE-cadherin using confocal microscopy, flow cytometry, and western blotting. These results showed that CD31 and VE-cadherin expression levels were
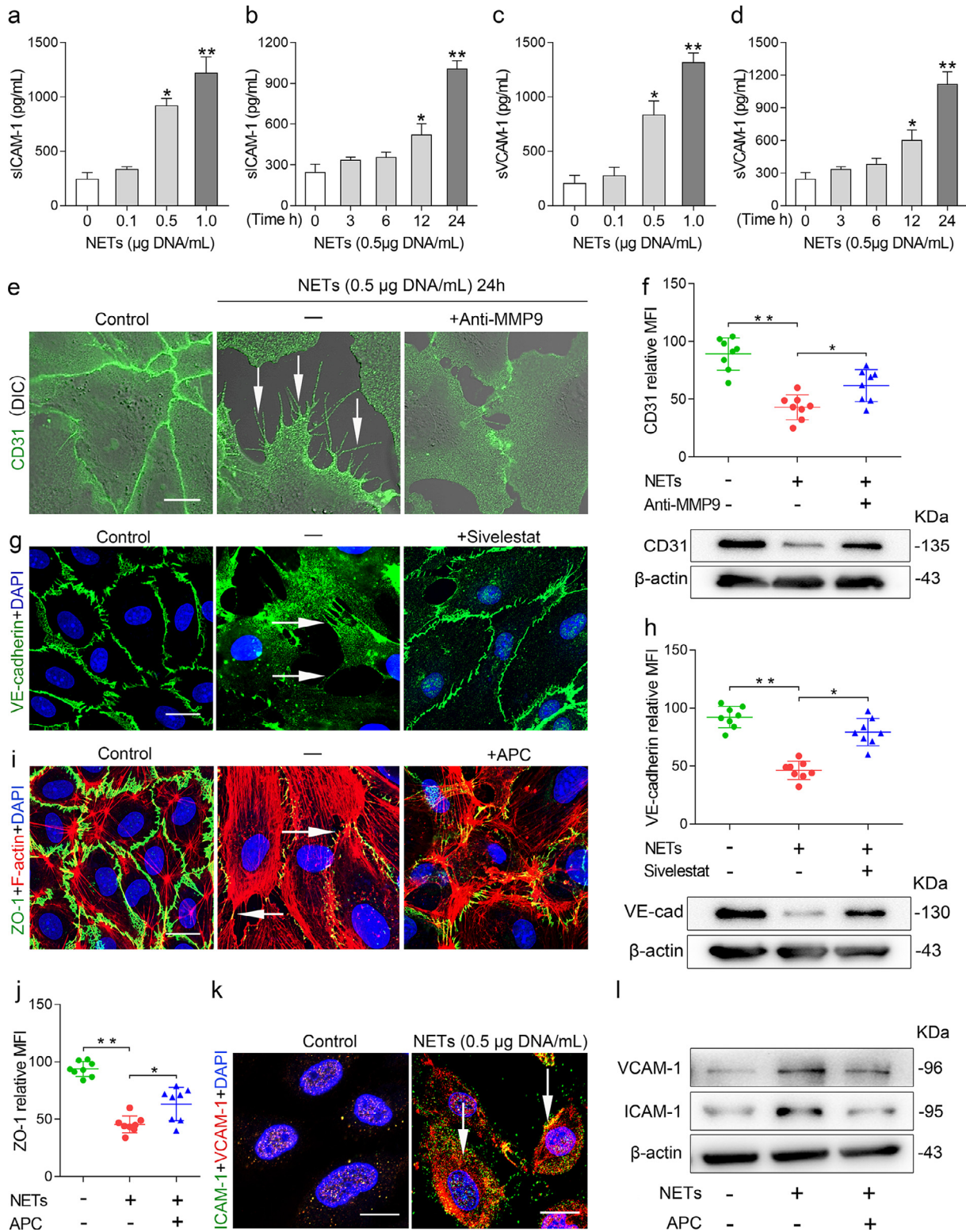
Fig. 6. The cytotoxic effect of NETs on HUVECs. (a-d) HUVECs were incubated with various concentrations of NETs or with NETs (0.5 µg DNA/mL) for the indicated periods of time. ICAM-1 and VCAM-1 expression were measured using ELISA. The expression of CD31, VE-cadherin, and ZO-1 on HUVECs is decreased after stimulation with NETs (0.5 µg DNA/mL) for 24 h, as determined by immunofluorescence imaging (e, g, i), flow cytometry (f, h upper panel and j, expression is indicated as mean fluorescence intensity [MFI]), and western blot analysis (f, h lower panel). Confocal microscopy images clearly showed the retraction of cell margins and extension of filopodia (arrows) indicating that endothelial cell-cell contacts are compromised. NETs invoked centralised F-actin bundles indicating actin stress fiber formation. For inhibition assays, HUVECs were incubated with NETs in the presence or absence of anti-MMP9 antibody, sivelestat, or APC, respectively. (k) Representative Confocal microscopy observation showed that the ICAM-1 (red) and VCAM-1 (green) were distributed in HUVECs surface (arrows). (l) ICAM-1 and VCAM-1 protein expression were tested by western blot analysis. Each point represents mean ± SD. One representative out of eight (e, g, i) or six (k) independent experiments is shown. Statistics, one-way ANOVA or Student's t-test. $*P < 0.05$, $**P < 0.01$. Scale bar: 5 µm. $*P < 0.05$, $**P < 0.01$ versus control in (a−d). For (a−d) $n = 10$. For (f) (h) (j) $n = 8$. (For interpretation of the references to colour in this figure legend, the reader is referred to the web version of this article.)

diminished in the NET-treated ECs compared with the control group. CD31 and VE-cadherin are known as the substrates of MMP9 and NE, respectively. We then estimated whether the decreases in these junctional proteins could be prevented by inhibiting the activity of MMP9 or NE. As shown in Fig. 6e−h, the pretreatment of NETs with anti-MMP9 antibody or sivelestat (a selective inhibitor of elastase) reduced the NET-induced loss of CD31 or VE-cadherin expression, respectively. To further illustrate the specificity of the sivelestat and anti-MMP9, we performed a cross experiment. As shown in Supplemental Fig S6, the pretreatment of NETs with sivelestat did not abolish the NET-induced loss of CD31 expression. Similarly, the inhibition of MMP9 with anti-MMP9 antibody did not significantly alter endothelial VE-cadherin expression levels.

To further investigate the effect of histones, we also examined their effects on the cell-cell junction and the endothelial actin cytoskeleton. The stimulation of HUVECs with NETs caused the rapid thinning of the tight junction protein ZO-1 at cell-cell borders and an increased number of F-actin stress fibers compared with the control treatment. The pretreatment of NETs with APC decreased NET-mediated cytotoxicity (Fig. 6i, j). Compared with the unstimulated controls, cells treated with NETs exhibited higher VCAM-1 and ICAM-1 expression, and the addition of APC abolished this function (Fig. 6k and l). These results suggest that the presence of NET-associated proteases and histones disturbs the endothelial monolayer integrity and propagates endothelial dysfunction.

3.8. NETs convert HUVECs to a procoagulant phenotype

To better understand EC thrombogenicity after treatment with NETs, we examined the expression of TF and PS on ECs. Immunofluorescence staining showed that HUVECs retracted from the cell-cell borders and formed filopodia and TF were dotted on the surface and filopodia of ECs. HUVECs exhibited irregular morphology and formed pseudopodia with intense green fluorescence after staining with lactadherin indicating that there was PS exposure. (Fig. 7a). TF mRNA expression increased rapidly after 12 h and reached its peak value at 24 h. The pretreatment of NETs with sivelestat, anti-MMP9 antibody, and APC abolished the expression of TF (Fig. 7b). Flow cytometry assays demonstrated that the PS exposure on HUVECs increased in a time-dependent manner upon incubation in the presence of NETs, rapidly increasing after 12 h and reaching a maximum at 24 h (Fig. 7c). The PS exposure on HUVECs was inhibited by 25% with sivelestat, by 39% with anti-MMP9 antibody, and by 52% with APC (Fig. 7c).

We next tested whether the expression of TF and PS supported elevated tenase and prothrombinase activity. Confocal microscopy showed the colocalisation of FVa and FXa on HUVECs treated with NETs, indicating that these cells provided many platforms for the binding of clotting factors, probably through PS and TF expression. FVa and FXa preferentially bound to filopodia and cell margins with high curvature (Fig. 7d). Furthermore, when HUVECs were treated with NETs, large fibrin strands with a radial distribution formed along their filopodia (Fig. 7d). These results showed that only HUVECs incubated with high NET concentrations showed an increased expression of FXa complexes and thrombin (Fig. 7e, $P < 0.01$). The production of FXa complexes and thrombin was reduced in the presence of sivelestat, anti-MMP9 antibody, or APC (Fig. 7f). Additionally, APC had a remarkable inhibitory effect compared with sivelestat or anti-MMP9 antibody (Fig. 7f, $P < 0.05$). Furthermore, a fibrin generation assay showed that the treatment of HUVECs with high NET concentrations triggered a more massive fibrin formation than in the other two groups (Fig. 7f). Sivelestat, anti-MMP9 antibody and APC effectively inhibited fibrin formation (Fig. 7g).

4. Discussion

All these results contributed to three significant findings. First, based on the blood samples collected from different locations, we demonstrated the local accumulation of PS-bearing NETs, activated PLTs, and PMPs at the site of carotid thrombosis. Moreover, the production of PS-bearing NETs follows a two-step procedure that needs both plasma from ICA occlusion patients and activated PLTs primarily present in the CLS. Second, PMPs can bind to NETs via histone-PS interactions; the accumulation of NET-PMP complexes provided an appropriate platform for coagulation factor deposition and played a crucial role in the thrombotic process. Third, NET-associated proteases and histones exerted a strong cytotoxic effect on ECs and augmented EC thrombogenicity through the induction of PS exposure and TF expression.

Increases in NET markers in the systemic blood of severe atherosclerosis and AIS patients have been reported [15,38]. Our study first reported that neutrophils assembled to the CLS during ICA occlusion became activated and released NETs, which were decorated with exposed PS. Moreover, in agreement with recent results on ischemic stroke thrombi [13,14,39], this work confirmed the presence of NET components in carotid thrombi and further demonstrated that neutrophils and NETs decorated with PS were present in thrombi. PS[+] MPs and blood cells serve as a necessary substrate for prothrombinase and tenase complexes in the coagulation cascade, thereby catalysing the generation of thrombin and the formation of fibrin [33,34]. We have previously informed that PS exposure on neutrophils in stroke supported significant increases in the generation of the FXa complex and thrombin formation [6]. This research goes beyond our previous studies, associating the release of neutrophil extracellular DNA and PS exposure from NETosis with increases in fibrin deposition and prothrombinase complex formation. NETs with functional PS can induce thrombin generation and PLT activation, leading to an increased risk of atherothrombosis.

In this study, we determined that the microenvironment in the circulation of ICA occlusion patients promotes PS exposure on neutrophils. In addition, PS upregulation was detected by culturing neutrophils with plasma from both the CLS and aortic samples of ICA occlusion patients in vitro. We imply that increased PS exposure on neutrophils may arise in part from the generation of plasma proinflammatory cytokines after stroke, including IL-1β and TNF-α, by macrophages [33,40]. At ischemic vascular lesions, local neutrophil-platelet interactions are likely to emerge as key players in NET formation [9,16,30]. In the present study, increased levels of activated PLTs and higher numbers of platelet-neutrophil aggregates were observed in the blood samples from the culprit carotid artery. Moreover, in agreement with a previous report [9], PLT activation by CLS-derived plasma was thrombin-dependent. Therefore, we proposed a "two-step" model for the pathogenesis of PS-bearing NETs in ICA occlusion: inflammatory stimuli of plasma increase the PS exposure of neutrophils; meanwhile, neutrophils interact with activated PLTs to stimulate the release of PS-expressing NETs in the local microenvironment around culprit lesions. As some researchers have identified the involvement of NETs in thrombotic formation through prothrombotic mediators, including TF, Factor XII, MPs, vWF and fibrinogen [9,10,41,42], we need to uncover the possible interactions of these molecules with PS on the NET scaffold with more experiments.

Adhesion of MPs and coagulation factors to NETs was found to induce thrombin generation, fibrin deposition and thrombosis, which can block the microvasculature and lead to reduced perfusion and changes of microenvironment [10,28,42]. Previous research revealed that cancer cell-derived MPs bound to NETs, which formed early in their model of deep vein thrombosis (DVT) and played a key role in thrombotic formation [27]. These studies suggested that NETs can recruit MPs to the site of the thrombosis. Indeed, PMPs are most abundant in the blood circulation, representing approximately 70−90% of all circulating MPs [22,43]. In our study, PMP levels were significantly higher in blood samples collected from ICA occlusion patients. Besides, NETs provide a scaffold for PS[+] PMP adhesion, suggesting that the formation of NET-PMP complexes serve as an assembly site for the
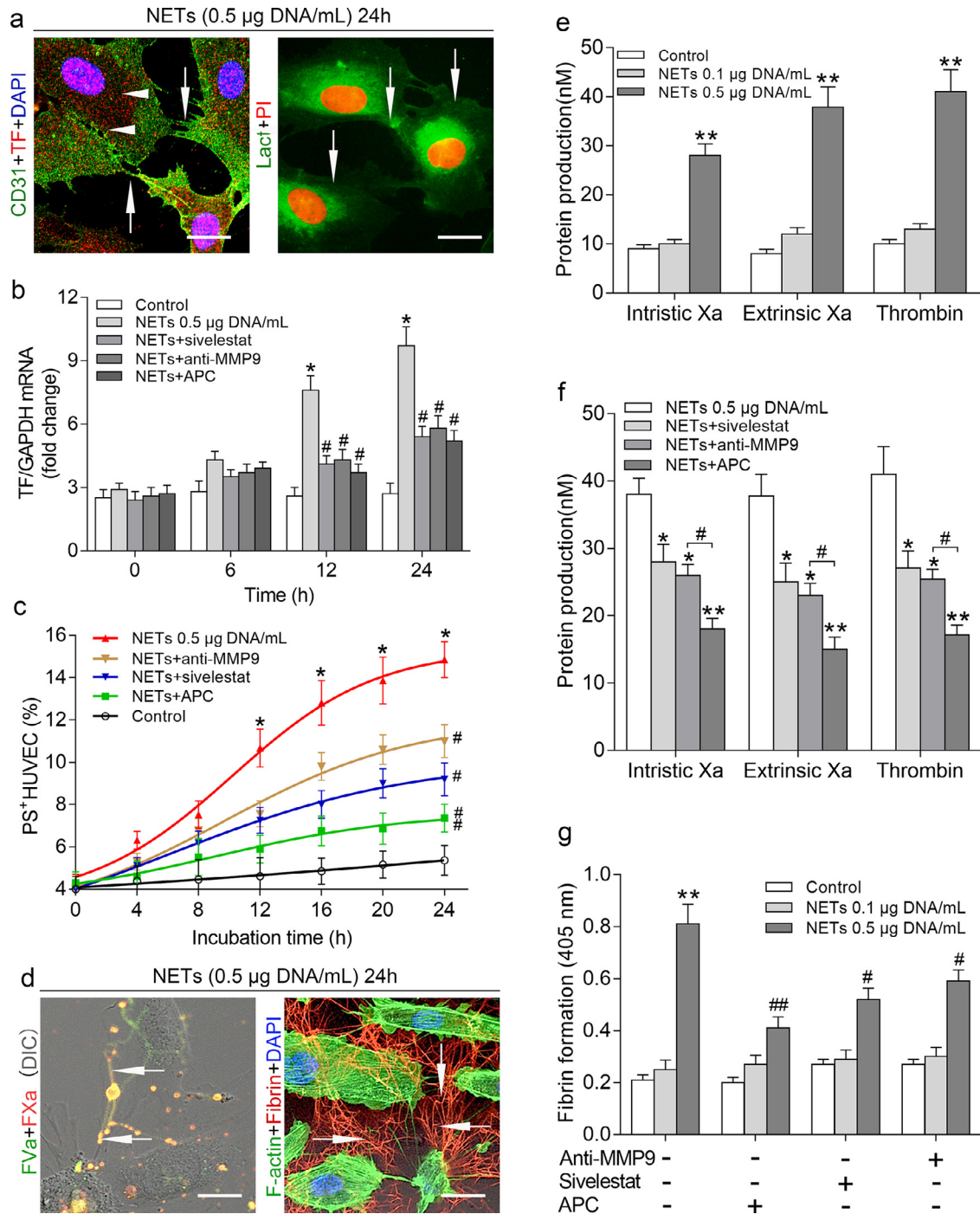
Fig. 7. NETs augment HUVECs thrombogenicity. (a) Representative confocal microscopy images showed that treatment of HUVECs with NETs (0.5 μg DNA/mL) for 24 h led to the retraction of cell margins, the extension of filopodia (arrows), and TF (red) were dotted on the surface and filopodia of HUVECs (arrowheads). HUVECs were incubated with lactadherin (green) and PI (red). HUVECs exhibited irregular morphology and formed pseudopodia with strong green fluorescence stained by lactadherin (arrows). Kinetics of TF (b) and PS (c) exposure on HUVECs incubated with NETs (0.5 μg DNA/mL) and in the presence of inhibitors. (d) FVa and FXa colocalisation (yellow) is observed on filopodia (arrows) near the retracted edges of HUVECs. HUVECs pretreated with NETs and incubated with healthy plasma showed considerable fibrin strand formation arranged radially along with filopodia (arrows) to form a fibrin network. (e) Intrinsic Xa, extrinsic Xa, and thrombin production were measured on HUVECs treated with various concentrations of NETs. (f) Inhibition assays of protein production were performed using sivelestat, anti-MMP9 antibody, or APC to degrade NET-associated elastase or histones before incubation with HUVECs. (g) Fibrin formation of HUVECs stimulated with various concentrations of NETs for 24 h in the presence of sivelestat, anti-MMP9 antibody, or APC was measured. Each point represents mean ± SD. Scale bar: 5 μm. One of six (a and d) independent experiments is shown. Statistics, one-way ANOVA or Student's t-test. $^*P < 0.05$ versus control, $^\#P < 0.05$ versus NETs (0.5 μg DNA/mL) group in (b) $^*P < 0.001$ versus control groups; $^\#P < 0.05$, $^{\#\#}P < 0.01$ versus NETs groups in (c). $^{**}P < 0.01$ versus control or NETs groups (0.1 μg DNA/mL) in (e) and (g). $^*P < 0.05$, $^{**}P < 0.01$ versus NETs groups in (f). $^\#P < 0.05$, $^{\#\#}P < 0.01$ versus sivelestat (-) anti-MMP9 antibody (-) APC (-) groups in (g). For (b) (c) (e) (f) (g) $n = 8$. (For interpretation of the references to colour in this figure legend, the reader is referred to the web version of this article.)

prothrombinase complex and promote thrombin generation. These results are in accordance with current research that showed the high-affinity binding of neutrophil-derived MPs (NMPs) to NETs *in vitro* [42]. An interesting finding was that coincubation with lactadherin

abolishes the attachment of PMPs to NETs, indicating that PS presented on PMPs mediates NET-PMP adhesion. Since PS can bind to histones [44,45], we assumed that histones derived from NETs could serve as ligands for PMP-expressed PS. Indeed, the degradation of histones

with APC reduced the binding of PMPs to NETs by 64.3%. Moreover, NETs also contain other proteins, which might facilitate PMP-NET interactions or endothelial injury.

Recent studies show that fibrinogen, extracellular DNA, and vWF form a co-localized network inside the thrombus in various inflammatory and thrombotic diseases, such as DVT and AIS [10,13]. In the present study, we showed that NETs decorated with PS were present in the carotid thrombus. We also provided clear evidence that PS-bearing NETs supported coagulation factor deposition around extracellular chromatin and accessible PS. A recent study confirms these results [28]. Therefore, NET formation and PS exposure play a vital role in atherothrombosis. Our research showed that NET structures might serve as a scaffold for the assembly of prothrombin, fibrinogen and Factor X, providing a rational scheme for the targeted inhibition of NETs and/or PS to reduce atherothrombosis. Of particular interest, we also provide direct evidence that NET-PMP complexes around the CLS in ICA occlusion patients induce thrombin generation and fibrin formation. This PCA could be decreased using DNase I and/or lactadherin while neutralizing anti-TF antibody had minimal effect. One plausible interpretation is that exposed TF in plasma is frequently encrypted with little or no measurable PCA [46].

Before the onset of atherosclerosis or thrombosis, vascular endothelium undergoes proinflammatory changes, such as aberrant activation or apoptosis, resulting in the loss of vascular integrity. Neutrophils and released NETs are responsible for the early response to endothelial injury and alter the anticoagulant function of ECs [21]. A recent study suggested that neutrophils and NETs contributed to local arterial EC activation, triggered TF activity and thrombin generation, and fostered clot formation [20]. However, the underlying mechanism is still not completely known. Here, we found that NETs from the CLS of ICA occlusion patients can lead to endothelial injury by eliciting EC activation and promoting adhesivity, which in turn increase further neutrophils aggregation to the plaque sites. Furthermore, we demonstrate that NETs induced the expression of PS and TF on HUVECs and elicited them to a procoagulant phenotype. Procoagulant ECs can provide many binding sites for the clotting factors, probably through the expression of PS and TF. Similar procoagulant activity in apoptotic ECs has been demonstrated in previous research [47], consistent with our findings.

NET-associated proteases, including MMP9 and NE, play a vital role in the elimination of extracellular matrix (ECM) to which the endothelial cells attach [48]. Disruption of this substrate could also promote EC activation or apoptosis. Here, we found that inhibiting the activity of NE and MMP9 could prevent the NET-induced loss of VE-cadherin and CD31 expression, respectively. These studies are supported by current research [31,49]. However, whether NET-associated proteases influence the effect of apoptotic ECs remains controversial. Pieterse et al. showed that the loss of endothelial intercellular contacts was not the result of NET-mediated endothelial apoptosis as measured by annexin V [31], which is inconsistent with other findings [50,51]. In addition, recent studies demonstrated that NET-associated histones promoted a rapid loss of endothelial intercellular contacts and induced ECs apoptosis or death [26,52], while APC can cleave and detoxify extracellular histones, consistent with our research. Our results also showed that sivelestat, anti-MMP9 antibody, and APC inhibit the cytotoxic effects of NET to protect ECs and decrease PCA, suggesting their critical role in preventing thrombotic complications in atherosclerosis.

In summary, this study described a novel mechanism for hypercoagulability and acute thrombotic complications in AIS patients with ICA occlusion. Although AIS patients received timely dual antiplatelet therapy, the PCA was still highly enhanced. Therefore, antiplatelet treatment alone is not enough to entirely prevent thrombophilia. Future therapeutic strategies could focus on combined strategies directed against NETs with classical antiplatelet drugs to further reduce the risk of thrombosis and to allow lower doses of antiplatelet drugs with fewer haemorrhagic complications.

Authors' Contributions

Conceptualization, P.Z. and J.J.; methodology, T.L. and B.L.; software, Y.L.; validation, Q.S., J.T. and H.Z.; formal analysis, Z.L.; investigation, P.Z., and J.J.; resources, S.Z.; data curation, S.M.; writing-original draft preparation, P.Z.; writing-review and editing, S.H., J.S. and V.N.; visualization, T.L.; supervision, J.S.; project administration, S.H.; funding acquisition, S.H., J.S. and P.Z. All authors reviewed and approved the final version of the manuscript.

Declaration of Competing Interest

The authors declare no conflict of interest.

Supplementary materials

Supplementary material associated with this article can be found in the online version at doi:10.1016/j.ebiom.2020.102671.

References

[1] Hendrix P, Sofoluke N, Adams MD, et al. Risk factors for acute ischemic stroke caused by anterior large vessel occlusion. Stroke 2019;50:1074–80.

[2] Goyal M, Menon BK, van Zwam WH, et al. Endovascular thrombectomy after large-vessel ischemic stroke: a meta-analysis of individual patient data from five randomized trials. Lancet 2016;387:1723–31.

[3] Campbell BC, Mitchell PJ, Kleinig TJ, et al. Endovascular therapy for ischemic stroke with perfusion-imaging selection. N Engl J Med 2015;372:1009–18.

[4] Wannamethee SG, Whincup PH, Lennon L, Rumley A, Lowe GD. Fibrin D-dimer, tissue-type plasminogen activator, von willebrand factor, and risk of incident stroke in older men. Stroke 2012;43:1206–11.

[5] Carcaillon L, Alhenc-Gelas M, Bejot Y, Scarabin PY, et al. Increased thrombin generation is associated with acute ischemic stroke but not with coronary heart disease in the elderly three-city cohort study. Arterioscler Thromb Vasc Biol. 2011;31:1445–51.

[6] Yao Z, Wang L, Wu X, et al. Enhanced procoagulant activity on blood cells after acute ischemic stroke. Transl Stroke Res 2017;8:83–91.

[7] Johnston SC, Easton JD, Farrant M, et al. Clopidogrel and aspirin in acute ischemic stroke and high-risk TIA. N Engl J Med 2018;379:215–25.

[8] de Boer OJ, Li X, Teeling P, et al. Neutrophils, neutrophil extracellular traps and interleukin-17 associate with the organisation of thrombi in acute myocardial infarction. Thromb Haemost 2013;109:290–7.

[9] Stakos DA, Kambas K, Konstantinidis T, et al. Expression of functional tissue factor by neutrophil extracellular traps in culprit artery of acute myocardial infarction. Eur Heart J 2015;36:1405–14.

[10] Fuchs TA, Brill A, Duerschmied D, et al. Extracellular dna traps promote thrombosis. Proc Natl Acad Sci USA 2010;107:15880–5.

[11] Zhu B, Liu H, Pan Y, et al. Elevated neutrophil and presence of intracranial artery stenosis increase the risk of recurrent stroke. Stroke 2018;49:2294–300.

[12] Boisseau W, Desilles JP, Fahed R, et al. Neutrophil count predicts poor outcome despite recanalization after endovascular therapy. Neurology 2019;93:e467–75.

[13] Staessens S, Denorme F, François O, et al. Structural analysis of ischemic stroke thrombi: histological indications for therapy resistance. Haematologica 2019;105:498–507.

[14] Laridan E, Denorme F, Desender L, et al. Neutrophil extracellular traps in ischemic stroke thrombi. Ann Neurol 2017;82:223–32.

[15] Valles J, Lago A, Santos MT, et al. Neutrophil extracellular traps are increased in patients with acute ischemic stroke: prognostic significance. Thromb Haemost 2017;117:1919–29.

[16] Maugeri N, Campana L, Gavina M, et al. Activated platelets present high mobility group box 1 to neutrophils, inducing autophagy and promoting the extrusion of neutrophil extracellular traps. J Thromb Haemost 2014;12:2074–88.

[17] McDonald B, Davis RP, Kim SJ, et al. Platelets and neutrophil extracellular traps collaborate to promote intravascular coagulation during sepsis in mice. Blood 2017;129:1357–67.

[18] Perdomo J, Leung HHL, Ahmadi Z, et al. Neutrophil activation and NETosis are the major drivers of thrombosis in heparin-induced thrombocytopenia. Nat Commun 2019;10:1322.

[19] Pertiwi KR, van der Wal AC, Pabittei DR, et al. Neutrophil extracellular traps participate in all different types of thrombotic and haemorrhagic complications of coronary atherosclerosis. Thromb Haemost 2018;118:1078–87.

[20] Folco EJ, Mawson TL, Vromman A, et al. Neutrophil extracellular traps induce endothelial cell activation and tissue factor production through interleukin-1alpha and cathepsin G. Arterioscler Thromb Vasc Biol 2018;38:1901–12.

[21] Franck G, Mawson TL, Folco EJ, et al. Roles of PAD4 and NETosis in experimental atherosclerosis and arterial injury: implications for superficial erosion. Circ Res 2018;123:33–42.

[22] Suades R, Padro T, Vilahur G, Badimon L. Circulating and platelet-derived microparticles in human blood enhance thrombosis on atherosclerotic plaques. Thromb Haemost 2012;108:1208–19.

[23] Najmeh S, Cools-Lartigue J, Giannias B, et al. Simplified human neutrophil extracellular traps (NETs) isolation and handling. J Vis Exp 2015;16.

[24] Sil P, Yoo DG, Floyd M, Gingerich A, Rada B. High throughput measurement of extracellular DNA release and quantitative NET formation in human neutrophils in vitro. J Vis Exp 2016;18.

[25] Yoo DG, Floyd M, Winn M, et al. NET formation induced by pseudomonas aeruginosa cystic fibrosis isolates measured as release of myeloperoxidase-DNA and neutrophil elastase-DNA complexes. Immunol Lett 2014;160:186–94.

[26] Saffarzadeh M, Juenemann C, Queisser MA, et al. Neutrophil extracellular traps directly induce epithelial and endothelial cell death: a predominant role of histones. PLoS ONE 2012;7:e32366.

[27] Thomas GM, Brill A, Mezouar S, et al. Tissue factor expressed by circulating cancer cell-derived microparticles drastically increases the incidence of deep vein thrombosis in mice. J Thromb Haemost 2015;13:1310–9.

[28] Healy LD, Puy C, Itakura A, et al. Colocalization of neutrophils, extracellular DNA and coagulation factors during NETosis: development and utility of an immunofluorescence-based microscopy platform. J Immunol Methods 2016;435:77–84.

[29] Campbell RA, Overmyer KA, Selzman CH, et al. Contributions of extravascular and intravascular cells to fibrin network formation, structure, and stability. Blood 2009;114:4886–96.

[30] Mangold A, Alias S, Scherz T, et al. Coronary neutrophil extracellular trap burden and deoxyribonuclease activity in ST-elevation acute coronary syndrome are predictors of ST-segment resolution and infarct size. Circ Res 2015;116:1182–92.

[31] Pieterse E, Rother N, Garsen M, et al. Neutrophil extracellular traps drive endothelial-to-mesenchymal transition. Arterioscler Thromb Vasc Biol 2017;37:1371–9.

[32] Abu Abed U, Brinkmann V. Immunofluorescence labelling of human and murine neutrophil extracellular traps in paraffin-embedded tissue. J Vis Exp 2019;10.

[33] Leventis PA, Grinstein S. The distribution and function of phosphatidylserine in cellular membranes. Annu Rev Biophys 2010;39:407–27.

[34] Vance JE, Steenbergen R. Metabolism and functions of phosphatidylserine. Prog Lipid Res 2005;44:207–34.

[35] Shi J, Gilbert GE. Lactadherin inhibits enzyme complexes of blood coagulation by competing for phospholipid-binding sites. Blood 2003;101:2628–36.

[36] Gao C, Xie R, Li W, et al. Endothelial cell phagocytosis of senescent neutrophils decreases procoagulant activity. Thromb Haemost 2013;109:1079–90.

[37] Kamińska A, Enguita FJ, Stępień EŁ. Lactadherin: an unappreciated haemostasis regulator and potential therapeutic agent. Vascul Pharmacol 2018;101:21–8.

[38] Borissoff JI, Joosen IA, Versteylen MO, et al. Elevated levels of circulating DNA and chromatin are independently associated with severe coronary atherosclerosis and a prothrombotic state. Arterioscler Thromb Vasc Biol 2013;33:2032–40.

[39] Farkas ÁZ, Farkas VJ, Gubucz I, et al. Neutrophil extracellular traps in thrombi retrieved during interventional treatment of ischemic arterial diseases. Thromb. Res. 2019;175:46–52.

[40] Lambertsen KL, Biber K, Finsen B. Inflammatory cytokines in experimental and human stroke. J Cereb Blood Flow Metab 2012;32:1677–98.

[41] Wvon Brühl ML, Stark K, Steinhart A, et al. Monocytes, neutrophils, and platelets cooperate to initiate and propagate venous thrombosis in mice in vivo. J Exp Med 2012;209:819–35.

[42] Wang Y, Luo L, Braun OO, et al. Neutrophil extracellular trap-microparticle complexes enhance thrombin generation via the intrinsic pathway of coagulation in mice. Sci Rep 2018;8:4020.

[43] Owens 3rd AP, Mackman N. Microparticles in hemostasis and thrombosis. Circ Res 2011;108:1284–97.

[44] Furnrohr BG, Groer GJ, Sehnert B, et al. Interaction of histones with phospholipids–implications for the exposure of histones on apoptotic cells. Autoimmunity 2007;40:322–6.

[45] Das R, Plow EF. Phosphatidylserine as an anchor for plasminogen and its plasminogen receptor, histone H2B, to the macrophage surface. J Thromb Haemost 2011;9:339–49.

[46] Chen VM, Hogg PJ. Encryption and decryption of tissue factor. J Thromb Haemost 2013;11(Suppl 1):277–84.

[47] Bombeli T, Karsan A, Tait JF, Harlan JM. Apoptotic vascular endothelial cells become procoagulant. Blood 1997;89:2429–42.

[48] Albrengues J, Shields MA, Ng D, Park CG, Ambrico A, Poindexter ME, et al. Neutrophil extracellular traps produced during inflammation awaken dormant cancer cells in mice. Science 2018;361.

[49] Kato H, Kuriyama N, Duarte S, et al. MMP-9 deficiency shelters endothelial PECAM-1 expression and enhances regeneration of steatotic livers after ischemia and reperfusion injury. J Hepatol 2014;60:1032–9.

[50] Florence JM, Krupa A, Booshehri LM, Allen TC, et al. Metalloproteinase-9 contributes to endothelial dysfunction in atherosclerosis via protease activated receptor-1. PLoS ONE 2017;12:e0171427.

[51] Grechowa I, Horke S, Wallrath A, et al. Human neutrophil elastase induces endothelial cell apoptosis by activating the PERK-CHOP branch of the unfolded protein response. FASEB J 2017;31:3868–81.

[52] Meegan JE, Yang X, Beard Jr RS, et al. Citrullinated histone 3 causes endothelial barrier dysfunction. Biochem Biophys Res Commun 2018;503:1498–502.